Journal of Alloys and Compounds 758 (2018) 72–77

Contents lists available at ScienceDirect

Journal of Alloys and Compounds

journal homepage: http://www.elsevier.com/locate/jalcom

Enhanced thermoelectric performance of $Bi_{0.4}Sb_{1.6}Te_3$ based composites with $CuInTe_2$ inclusions

Y.S. Wang [a, b], L.L. Huang [a, b], D. Li [a], J. Zhang [a], X.Y. Qin [a, *]

[a] Key Laboratory of Materials Physics, Institute of Solid State Physics, Chinese Academy of Sciences, 230031, Hefei, PR China
[b] University of Science and Technology of China, Hefei, 230026, PR China

ARTICLE INFO

Article history:
Received 21 December 2017
Received in revised form
18 April 2018
Accepted 3 May 2018
Available online 5 May 2018

Keywords:
Thermoelectric materials
$Bi_{0.4}Sb_{1.6}Te_3$
$CuInTe_2$
Composites
Hot pressing

ABSTRACT

$Bi_{0.4}Sb_{1.6}Te_3$ (BST) based composites incorporated with $CuInTe_2$ particles have been prepared and their thermoelectric properties were studied in the temperature range from 300 to 500 K. The results indicate that at 300 K the incorporation of 0.2 wt% CuInTe2 in BST causes 14% increase in power factor (PF) and 38% reduction in lattice conductivity simultaneously. As a result, a maximum $ZT = 1.45$ at 400 K is achieved in the composite sample with $f = 0.2$ wt%, which is ~45% larger than that of BST studied here. The enhancement of PF originates from the increase of both electrical conductivity due to increased hole concentration and thermopower via energy filtering effect. While, the reduction of the lattice thermal conductivity could be ascribed to enhanced phonon scattering at the interfaces and $CuInTe_2$ inclusions in the composite samples. Present results demonstrate that incorporation of a proper amount of $CuInTe_2$ in BST is an effective way to improving thermoelectric performance of BST alloys.

© 2018 Elsevier B.V. All rights reserved.

1. Introduction

Thermoelectric (TE) materials can realize the direct and reversible conversion of heat energy and electric energy [1,2]. The vital mean for TE materials to achieve higher energy conversion efficiency is to enhance the dimensionless figure of merit $ZT = \alpha^2 T/(\rho\kappa)$, where α, T, ρ and κ are the thermopower, absolute temperature, electrical resistivity and the total thermal conductivity [3], respectively. Among all the TE materials, $Bi_xSb_{2-x}Te_3$ (BST) alloys are the state-of-the-art thermoelectric materials near room temperature [4], and play an irreplaceable role in low-grade waste heat recovery and refrigeration [5].

So far, tremendous efforts have been devoted to improving the performance of p-type BST alloys, such as optimizing carrier concentration by adjusting the proportion of Bi and Sb [4,6,7] and decreasing the bipolar thermal conductivity by doping with Cu, Ag, Pd or Cd elements [8–10]. Specially, a lot of work shows that incorporation of a proper second nanophase in BST could improve its thermoelectric performance to a certain degree through lowering thermal conductivity in terms of phonon scattering of the dispersed particles [11–15]. However, our previous work [13–16] indicates that the degree of improvement of thermoelectric performance of BST and the optimized temperature range are closely related to the species of the second phases. Therefore, explorations of new BST based composite systems possess great significance to elevating thermoelectric performance of BST alloys.

In this work, we prepare BST based composites incorporated with $CuInTe_2$ nanoparticles. $CuInTe_2$ compound is a p-type semiconductor with a band-gap of 1.02eV [17,18], which is much larger than that of BST alloy (0.13–0.15eV). Hence, as $CuInTe_2$ particles are embedded in BST matrix, interface barriers will be formed which could give rise to energy filtering effect, leading to enhancement of thermopower. Moreover, the existence of massive $CuInTe_2$/BST interfaces will cause strong phonon scattering, resulting in drop of thermal conductivity. Indeed, our results show that the power factor (PF) of the composite samples f(CuInTe2)/BST ($f = 0.1$–0.3 wt %) increases. Specially, PF for sample with $f = 0.2$ wt% reaches 41 $\mu Wcm^{-1}K^{-2}$ (300 K) that is ~14% higher than that of BST. Other than the decrease of the electrical resistivity, this enhancement of PF is mainly ascribed to an enhancement of thermopower due to energy filtering effect. Moreover, The lattice thermal conductivity decreases monotonously with increasing content of $CuInTe_2$ and as $f = 0.2$ wt% it reaches 0.42 $Wm^{-1}K^{-1}$ (at 300 K) that is around 38% lower than that of BST. As a result, a maximum $ZT = 1.45$ at 400 K is achieved in the composite sample with $f = 0.2$ wt%, which is ~45% larger than that of BST.

* Corresponding author.
E-mail address: xyqin@issp.ac.cn (X.Y. Qin).

https://doi.org/10.1016/j.jallcom.2018.05.035
0925-8388/© 2018 Elsevier B.V. All rights reserved.

2. Experimental

2.1. Synthesis and test

High purity elements, Bi (99.995%), Sb (99.999%), Te (99.99%) were weighed by stoichiometry $Bi_{0.4}Sb_{1.6}Te_3$, and then sealed in evacuated quartz ampoules under vacuum of 10^{-3} Pa. The sealed ampoules were subsequently heated up to 1073 K at a rate of 1 K per minute and then soaked at this temperature for 10 h. The method for synthesis of $CuInTe_2$ was the same as BST, but the soaking temperature of $CuInTe_2$ was 100 K higher than that of BST. To prepare $CuInTe_2$ nanoparticles, the obtained ingot was ground into powders by hands, then milled the coarse $CuInTe_2$ powders to smaller size by vibration ball-milling machine. The $CuInTe_2$ and BST powders were mixed in a mortar for 1 h in accordance with the weight ratios of 0.1%, 0.2% and 0.3%. Finally, the bulk samples were obtained by hot-pressing the composite powder under a pressure of 600 MPa in a vacuum at 673 K for 1 h.

The phase structure of the obtained samples was studied by X-ray diffraction (Philips diffractometer, Cu Kα radiation) at different scanning rates of (2θ =) 20°/min and 2°/min, respectively, at room temperature. The morphology and fractographs were observed by field emission scanning electron microscopy (FE-SEM). Electrical resistivity and the thermopower were measured using a thermopower/electric resistance measuring system (ZEM-3, Ulvac-Riko, Japan). The thermal diffusivity D was measured using the laser flash method (Netzsch, LFA-457). Due to the anisotropic characteristics of BST alloys, D was measured in the direction perpendicular to the pressing direction, ensuring that the thermal and electrical properties were measured in the same direction. For this purpose, large flaky samples with their normal being perpendicular to pressing direction were cut from the large cylinder samples of the size Φ13 × 10 mm. The specific heat C_p refers to our previous work [10]. The density d was measured by Archimedes' method. The total thermal conductivity was calculated from the measured thermal diffusivity D, specific heat C_p, and density d according to the relationship $\kappa = DdC_p$. The Hall coefficient was measured at 300 K using the Van der Pauw method.

2.2. Material characterization

The XRD patterns for BST, $CuInTe_2$ and $f(CuInTe_2)$/BST composite samples (f = 0.1, 0.2, and 0.3 wt%) are shown in Fig. 1. One can see that the main diffraction peaks for f ($CuInTe_2$)/BST composite samples (f = 0.1, 0.2, and 0.3 wt%) correspond to the patterns of BST, which are consistent with its standard PDF card (JCPDS#01-072-1836). Although the diffraction peaks from $CuInTe_2$ phase have not been observed in the fast scanning XRD patterns of the composite samples due to its small contents in the composite samples, $CuInTe_2$ phase can be detected in the slow scanning XRD patterns (obtained at the scanning rate of 2°/min), as is shown in the inset of Fig. 1. The peak marked with a diamond in curve (a) of the inset is (112) diffraction peak for $CuInTe_2$, indicating its existence in the composite samples. In addition, the existence of $CuInTe_2$ nanoparticles was also confirmed by our FE-SEM microstructure analysis.

Fig. 2 (a) gives FE-SEM image for the fracture surface of BST matrix, from which one can see micron-sized particles with layered structure; In contrast, in the fracture surface of composite sample with f = 0.3 wt% $CuInTe_2$ inclusions, one can find small particles with the size in about 10–300 nm (Fig. 2(b)), which is consistent with the statistical analysis of size distribution of the $CuInTe_2$ particles (Fig. 2(d)), suggesting that these small particles belong to $CuInTe_2$ phase. It is true that our element mapping with EDS shows that these particles correspond to indium rich and Te/Sb deficient regions (Fig. 2(e)), confirming these particles are dispersed $CuInTe_2$ phase. Present results indicate that $CuInTe_2$ particles are incorporated in BST matrix and $CuInTe_2$/BST nanocomposite samples are successfully prepared.

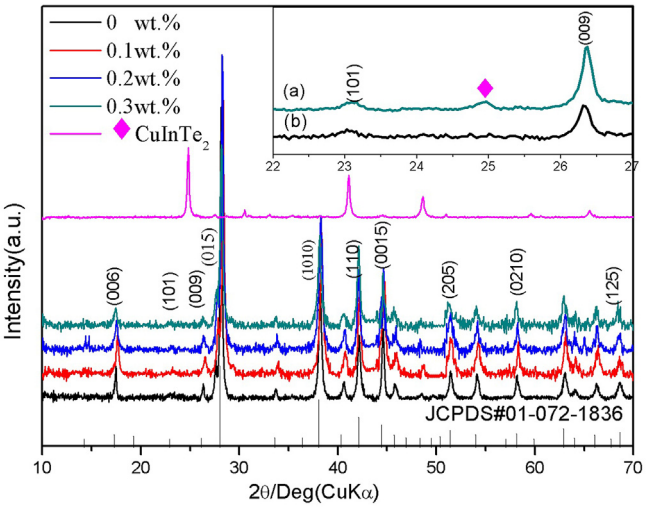

Fig. 1. Room temperature XRD patterns for $f(CuInTe_2)$/BST (f = 0, 0.1, 0.2 and 0.3 wt%). The inset shows the XRD patterns obtained at scanning rate (2θ) of 2°/min for BST (a) and composite samples with f = 0.3 wt% (b).

3. Results and discussion

3.1. Electrical resistivity and thermopower

The temperature dependence of electrical resistivity (ρ) and thermopower (α) of $f(CuInTe_2)$/BST composite samples (f = 0.1, 0.2, and 0.3 wt%) are shown in Fig. 3. It can be seen from Fig. 3(a) that ρ increases with increasing temperature for all samples, indicating that they all exhibit a degenerate semiconductor behavior. In addition, the inclusion of $CuInTe_2$ causes decreases in ρ significantly in the all temperature range investigated. For instance, ρ at 300 K decreases from 1.32 to 1.14, 0.76 and 0.56 Ω m as f increase from 0 to 0.1, 0.2 and 0.3 wt%, respectively.

On the other hand, the α value increases with increasing temperature, and then decreases as the temperature increase further, leaving a maximum (α_{max}) on the α-T curve at T_p = 375 K, 400 K, 425 K and 450 K for the composite samples with f = 0, 0.1, 0.2 and 0.3 wt%, respectively, as shown in Fig. 3 (b). The upshift in α_{max} to higher temperatures suggests that the bipolar contribution to the electrical conduction occurs at a relatively higher temperatures [19]. Obviously, the decrease of α at $T > T_p$ can be ascribed to bipolar conduction (i.e. intrinsic thermal excitation of carriers). In particular, one can see that α of composite samples drops with increasing f and is smaller than that of BST in the low temperature ranges (T<~380 K-480 K, where concrete value of T depends on $CuInTe_2$ content f, as shown in Fig. 3(b)), beyond which α of the composite sample is obviously larger than that of BST. According to Mott formula [16], α is related to carrier concentration p as following:

$$\alpha = \frac{\pi^2 k_B^2 T}{3q}\left[\frac{\partial \ln(\sigma(E))}{\partial E}\right]_{E=E_f} = \frac{\pi^2 k_B^2 T}{3q}\left[\frac{1}{p}\frac{\partial p(E)}{\partial E} + \frac{1}{\mu}\frac{\partial \mu(E)}{\partial E}\right]_{E=E_f} \quad (1)$$

with carrier mobility $\mu(E) = q\tau/m^*$, where σ is the electrical conductivity, q the carrier charge, k_B the Boltzmann constant, m^* the effective mass and E_f the Fermi energy. Assuming energy bands

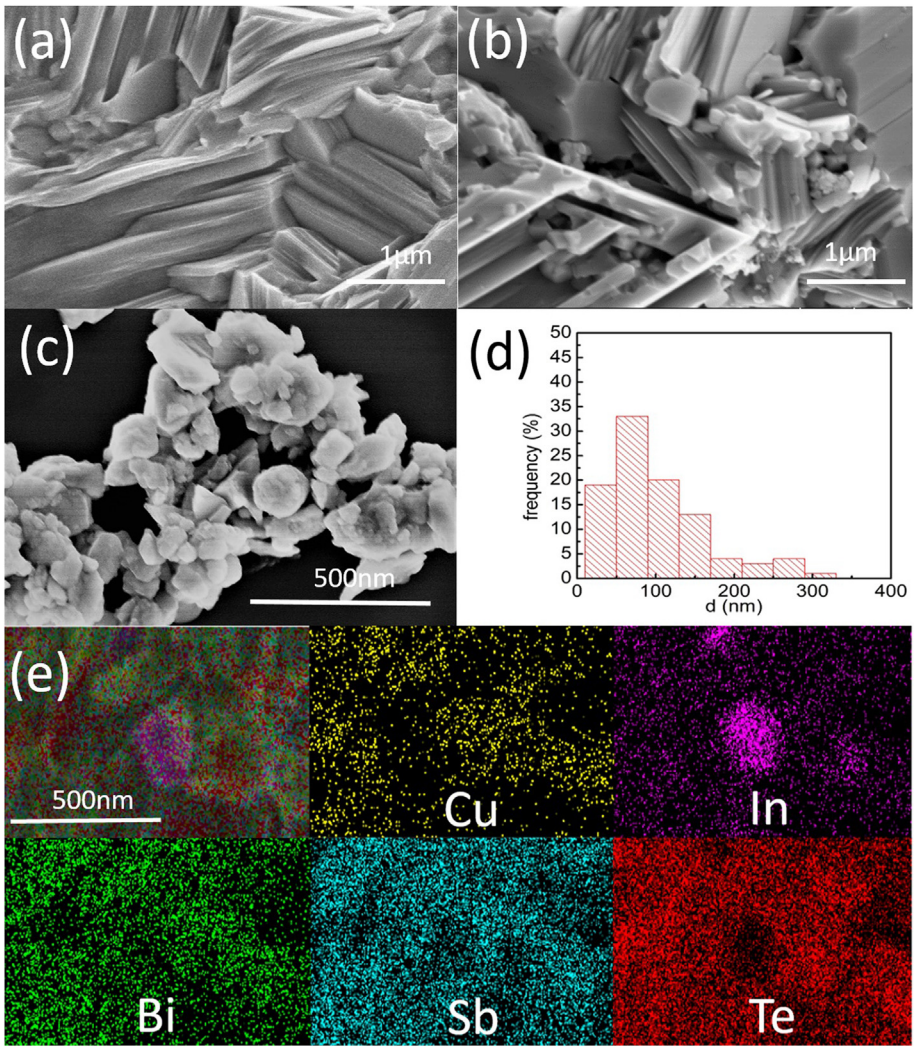

Fig. 2. FE-SEM images of (a) the fraction surface for BST, (b) fraction surface for f ($CuInTe_2$)/BST ($f = 0.3$ wt%) composites, (c) FE-SEM micrograph of $CuInTe_2$ particles. (d) Statistical analysis result of size distribution of the particles in (c). (e) EDS analysis of the elements Cu, In, Bi, Sb and Te.

have a parabolic dispersion relation, $\tau(E)$ usually has power form with energy E, i.e. $\tau(E) = \tau_0 E^{\lambda-1/2}$ [20].

Then, equation (1) can be expressed as:

$$\alpha = \frac{\pi^2 k_B^2 T}{3q}\left[\frac{1}{p}\frac{\partial p(E)}{\partial E} + \frac{\lambda - \frac{1}{2}}{E}\right]_{E=E_f} \tag{2}$$

where λ is scattering parameter. Formula (2) tells us that α decreases with increasing carrier concentration p. In fact, our Hall coefficient measurements indicate that p increases from 2.0 to $6.3 \times 10^{19} cm^{-3}$ (as given in Table 1) The increase of p could come from interface defects, such as vacancies, dangling bands and antisites defects, which qualitatively explains why α drops with increasing f. Similarly, the decrease of ρ with increasing f can be ascribed to the increase of carrier concentration p. However, it worthwhile to point it out that α increases with increase in scattering parameter λ, as shown in formula (2). In fact, according to single parabolic band model the thermopower and density of state effective mass m_d^* can be calculated as following [21]:

$$m_d^* = \frac{h^2}{2k_B T}\left(\frac{p}{4\pi F_{1/2}(\xi_F)}\right)^{2/3} \tag{3}$$

$$\alpha = \frac{k_B}{e}\left[\frac{(\lambda+2)F_{\lambda+1}(\xi_F)}{(\lambda+1)F_\lambda(\xi_F)} - \xi_F\right] \tag{4}$$

$$F_i(\xi_F) = \int_0^\infty \frac{x^i}{1 + e^{x-\xi_F}} dx \tag{5}$$

where h and ξ_F are the Planck constant and reduced Fermi level $E_f/(k_B T)$, respectively. Here, we assume that acoustic phonon scattering is dominant in BST ($\lambda = 0$ for the sample with $f = 0$), we obtain $m_d^* = 1.14 m_0$ (where m_0 is the free electron mass) for BST at 300 K. Moreover, in our calculations, it is assumed that m_d^* is a constant in all the specimens with different f. Then, one obtains λ values for all the specimens. As shown in Table 1, the values of λ increases in all composites specimens, indicating enhanced energy filtering effect (EFE) due to carrier scattering at the $CuInTe_2$/BST interfaces, which leads to ~14.5, ~19.3 and ~17 μV/K rise in α at 300 K for the specimens with $f = 0.1$, 0.2 and 0.3 wt%, respectively,

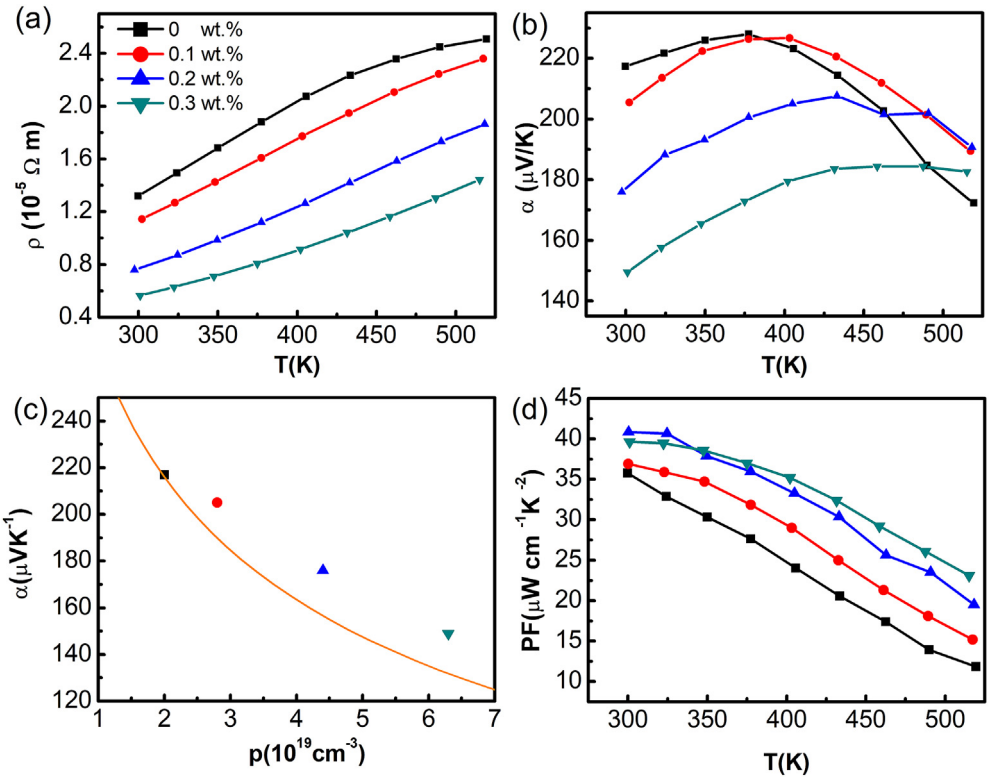

Fig. 3. Temperature dependencies of (a) electrical resistivity and (b) thermopower for f ($CuInTe_2$)/BST ($f = 0$, 0.1, 0.2 and 0.3 wt%). (c)The dependence of thermopower on carrier concentration (Pisarenko relation) at 300 K for BST (where corresponding α values for f ($CuInTe_2$)/BST specimens are also shown). (d)The variation of PF with temperature for f ($CuInTe_2$)/BST composite specimens ($f = 0$, 0.1, 0.2, and 0.3 wt%).

Table 1
A List of carrier concentration p, Hall mobility μ, Lorenz number L, scattering parameter λ (at 300 K), relative density d_r and ZT_{ave} for all samples.

f (wt%)	p ($10^{19}cm^{-3}$)	μ($cm^2V^{-1}s^{-1}$)	L ($10^{-8}V^2K^{-2}$)	λ_{300K}	d_r (%)	ZT_{ave}
0	2	230	1.60	0	97.9	0.92
0.1	2.8	197	1.65	0.2	97.0	1.2
0.2	4.4	185	1.72	0.24	98.1	1.32
0.3	6.3	182	1.79	0.23	98.2	1.2

Note: Relative density $d_r = d/d_0$ (here d is the measured density and d_0 is theoretical density of a material). d_0 for $Bi_{0.4}Sb_{1.6}Te_3$ is $d_{02} = 6.79$ g/cm^3. For a composite sample f(CuInTe2)/BST, its theoretical density d_{0c} is expressed as $\frac{1}{d_{0c}} = (1-f)\frac{1}{d_{02}} + f\frac{1}{d_{01}}$ (here d_{01} (=6.16 g/cm^3) is theoretical density of $CuInTe_2$). ZT_{ave} is average ZT in the temperature range from 300 to 500 K.

as shown in Fig. 3(c), where a Pisarenko relation (solid line) is given for BST. Due to the enhanced S from EFE and decrease of ρ (Fig. 3(a)), the PF for all the composite samples is increased in all the temperature range investigated. Specially, at 300 K PF increases by ~14% for sample with $f = 0.2\%$ as compared to BST, as shown in Fig. 3(d).

3.2. Thermal conductivity and thermoelectric performance

The temperature dependence of the total thermal conductivity κ_T of f ($CuInTe_2$)/BST composite samples ($f = 0.1$, 0.2, and 0.3 wt%) are shown in Fig. 4(a). κ_T value decreases with increasing $CuInTe_2$ inclusion, and then increases as $CuInTe_2$ content increases further. On the other hand, a minimum on each κ_T-T curve occurs at $T_m = 350$ K, 400 K, 425 K and 450 K for the composite samples with $f = 0$, 0.1, 0.2 and 0.3 wt%, respectively. These extremes and the peaks of thermopower are all related to thermal excitation of minorities. T_m is roughly consist with T_p which is mentioned above.

Both electrons and holes contribute to the thermal/electrical transport in a narrow-gap semiconductor at high temperature, leading to bipolar effect in the high temperature region [22]. Thus, the total thermal conductivity must be written in the following form: $\kappa_T = \kappa_L + \kappa_C + \kappa_b$, where κ_T is the total thermal conductivity, κ_L the lattice thermal conductivity, κ_C the carrier thermal conductivity and κ_b the bipolar thermal conductivity [4,10,23]. κ_C can be estimated by the Wiedemann–Franz relation ($\kappa_C = LT/\rho$), in which the Lorenz number L is estimated using formula (5) with the assumption of transport dominated by acoustic scattering and a single parabolic band [24].

$$L = \left(\frac{k_B}{e}\right)^2 \frac{3F_0(\xi_F)F_2(\xi_F) - 4F_1(\xi_F)^2}{F_0(\xi_F)^2} \quad (5)$$

The calculated values ($1.6–1.79 \times 10^{-8}V^2K^{-2}$) of L for different samples are listed in Table 1. Therefore, one can obtain ($\kappa_L + \kappa_b$) by subtracting κ_C from κ_T, as shown in Fig. 4(b). We extrapolate the κ_L value by fitting the points of ($\kappa_L + \kappa_b$) at the range of 300 K–350 K according to the relationship of $\kappa_L \propto 1/T$, as is presented in Fig. 4(b) by dot line. κ_L decreases monotonously with increasing content of $CuInTe_2$ inclusions due to enhanced phonon scattering in the composite samples, and it reaches 0.42 $Wm^{-1}K^{-1}$ (at 300 K) that is around 38% lower than that of BST. According to the Debye-Callaway model, the total phonon relaxation time is a reciprocal sum of the relaxation times of the pertinent scattering mechanisms and κ_L can be expressed as following [25]:

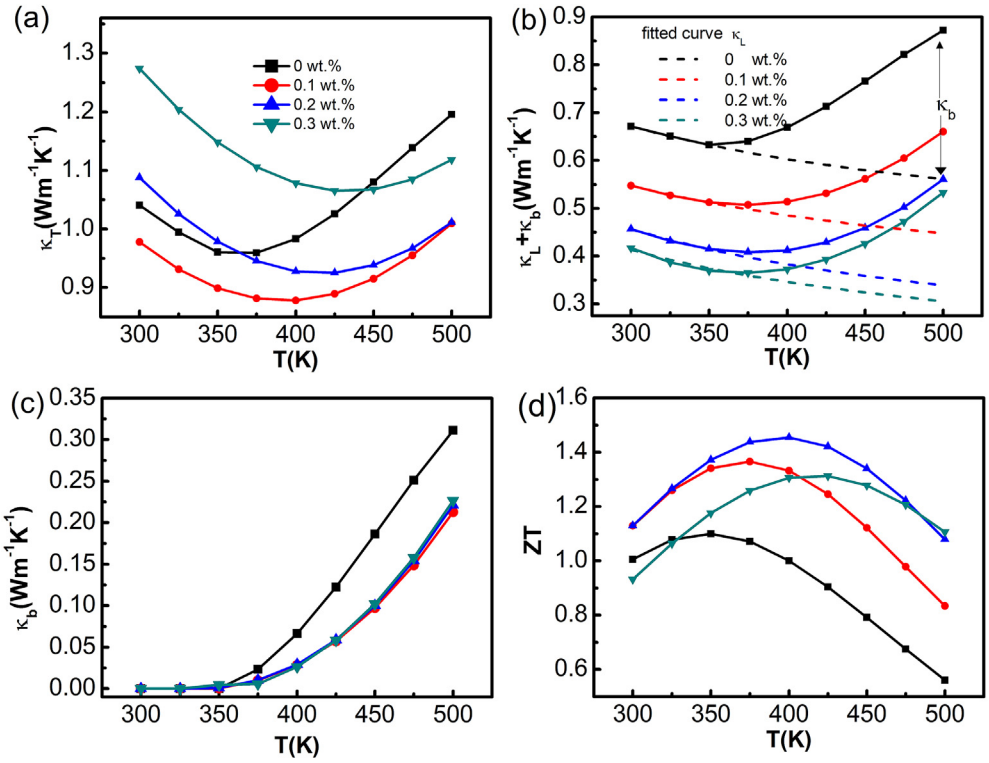

Fig. 4. Temperature dependences of (a) thermal conductivity, (b) ($\kappa_L+\kappa_b$), (c) bipolar thermal conductivity κ_b and (d) ZT for f ($CuInTe_2$)/BST composite simples (f = 0, 0.1, 0.2, and 0.3 wt%).

$$\kappa_L = \frac{4\pi k_B^4 T^3}{\upsilon h^3} \int_0^{\theta_D/T} \tau \frac{z^4 \exp(z)}{[\exp(z)-1]^2} dz \quad (6)$$

where k_B is the Boltzmann constant, h is Plank's constant, υ is the average sound velocity, θ_D is Debye temperature, τ is total phonon relaxation time, and z is reduced phonon frequency. The three dominant scattering mechanisms relevant to all BST polycrystalline samples are Umklapp phonon-phonon scattering, point defect scattering and boundary scattering [25]. Because of the existence of second phase, the additional phonon scattering from nano-inclusions and formed phase boundaries should take place, leading to decrease of thermal conductivity. In fact, the total phonon relaxation time for composite samples can be written as:

$$\tau^{-1} = \tau_U^{-1} + \tau_{PD}^{-1} + \tau_B^{-1} + \tau_{NP}^{-1} + \tau_{IF}^{-1} \quad (7)$$

where τ_U, τ_{PD} and τ_B are the relaxation times corresponding to scattering from the Umklapp, point defect and boundary, respectively. τ_{NP} and τ_{IF} are the relaxation times corresponding to additional phonon scattering from nanoinclusions and formed phase boundaries.

As shown in Fig. 4 (b), the deviations of the data from dot lines is the bipolar contribution to thermal conductivity. The maximum κ_b value is reduced to 0.22 Wm^{-1}K^{-1} at 500 K for the composite materials, which is around 29% lower than that of BST. This suppression of bipolar thermal conduction can be mainly ascribed to the interface scattering of the minorities. As a result, the ZT values have been improved in different degrees for composite simples, as shown in Fig. 4(d). Especially, a maximum ZT = 1.45 at 400 K is achieved in the composite sample with f = 0.2 wt%, which is ~45% larger than that of $Bi_{0.4}Sb_{1.6}Te_3$ matrix. Furthermore, the average ZT (ZT_{ave}) is raised to 1.32 in the composite sample with f = 0.2 wt%, as shown in Table 1, which is ~43% larger than that of BST.

4. Conclusions

In summary, the thermoelectric properties of $Bi_{0.4}Sb_{1.6}Te_3$ based composites incorporated with $CuInTe_2$ particles were investigated in the temperature range from 300 to 500 K. The results indicate that the addition of proper amounts of $CuInTe_2$ can elevate both electrical conductivity through increasing carrier concentration and thermopower via energy filtering effect. Meanwhile, the lattice thermal conductivity is reduced due to enhanced phonon scattering by the interfaces and $CuInTe_2$ inclusions. Specifically, incorporation of 0.2 wt% CuInTe2 in BST causes 14% increase in power factor (PF) and 38% reduction in lattice conductivity at room temperature; as a result, a maximum ZT = 1.45 at 400 K is achieved, which is ~45% larger than that of BST studied here. Present results demonstrate that incorporation of a proper amount of $CuInTe_2$ in BST is an effective way to improving its thermoelectric performance.

Acknowledgements

We acknowledge the funding support from the Natural Science Foundation of China under grant Nos. 11674322, 51672278 and 11374306, Anhui Provincial Natural Science Foundation (No. 1608085MA17).

References

[1] B. Xu, T. Feng, M.T. Agne, L. Zhou, X. Ruan, G.J. Snyder, Y. Wu, Highly porous thermoelectric nanocomposites with low thermal conductivity and high figure of merit from large-scale solution-synthesized Bi2 Te2.5 Se0.5 hollow nanostructures, Angew Chem. Int. Ed. Engl. 56 (2017) 3546–3551.

[2] T. Zhu, Y. Liu, C. Fu, J.P. Heremans, J.G. Snyder, X. Zhao, Compromise and synergy in high-efficiency thermoelectric materials, Adv. Mater. 29 (2017) 26.
[3] D.H. Kim, I.H. Kwon, C. Kim, B. Han, H.-J. Im, H. Kim, Tellurium-evaporation-annealing for p-type bismuth–antimony–telluride thermoelectric materials, J. Alloys Compd. 548 (2013) 126–132.
[4] L.P. Hu, T.J. Zhu, Y.G. Wang, H.H. Xie, Z.J. Xu, X.B. Zhao, Shifting up the optimum figure of merit of p-type bismuth telluride-based thermoelectric materials for power generation by suppressing intrinsic conduction, NPG Asia Mater. 6 (2014) e88.
[5] W. Xie, J. He, H.J. Kang, X. Tang, S. Zhu, M. Laver, S. Wang, J.R. Copley, C.M. Brown, Q. Zhang, T.M. Tritt, Identifying the specific nanostructures responsible for the high thermoelectric performance of (Bi,Sb)2Te3 nanocomposites, Nano Lett. 10 (2010) 3283–3289.
[6] D. Li, R.-r. Sun, X.-y. Qin, Improving thermoelectric properties of p-type Bi2Te3-based alloys by spark plasma sintering, Prog. Nat. Sci. Mater. Int. 21 (2011) 336–340.
[7] M. F.G. Serrano-Sanchez, N.M. Nemes, N. Biskup, M. Varela, J.L. Martinez, M.T. Fernandez-Diaz, J.A. Alonso, Enhanced figure of merit in nanostructured (Bi,Sb)2Te3 with optimized composition, prepared by a straightforward arc-melting procedure, Sci. Rep. 7 (2017) 6277.
[8] H. Li, H. Jing, Y. Han, Y. Xu, G.-Q. Lu, L. Xu, Microstructure and transport properties of copper-doped p-type BiSbTe alloy prepared by mechanical alloying and subsequent spark plasma sintering, J. Alloys Compd. 576 (2013) 369–374.
[9] D. Xie, J. Xu, Z. Liu, G. Liu, H. Shao, X. Tan, H. Jiang, J. Jiang, Stabilization of thermoelectric properties of the Cu/Bi0.48Sb1.52Te3 composite for advantageous power generation, J. Electron. Mater. 46 (2016) 2746–2751.
[10] F. Hao, P. Qiu, Y. Tang, S. Bai, T. Xing, H.-S. Chu, Q. Zhang, P. Lu, T. Zhang, D. Ren, J. Chen, X. Shi, L. Chen, High efficiency Bi2Te3-based materials and devices for thermoelectric power generation between 100 and 300 °C, Energy Environ. Sci. 9 (2016) 3120–3127.
[11] T. Zhang, J. Jiang, Y. Xiao, Y. Zhai, S. Yang, G. Xu, In situ precipitation of Te nanoparticles in p-type BiSbTe and the effect on thermoelectric performance, ACS Appl. Mater. Interfaces 5 (2013) 3071–3074.
[12] B. Xu, M.T. Agne, T. Feng, T.C. Chasapis, X. Ruan, Y. Zhou, H. Zheng, J.H. Bahk, M.G. Kanatzidis, G.J. Snyder, Y. Wu, Nanocomposites from solution-synthesized PbTe-BiSbTe nanoheterostructure with unity figure of merit at low-medium temperatures (500-600 K), Adv. Mater. 29 (2017) 1605140.
[13] Y.Y. Li, X.Y. Qin, D. Li, J. Zhang, C. Li, Y.F. Liu, C.J. Song, H.X. Xin, H.F. Guo, Appl. Phys. Lett. 108 (2016), 062104.
[14] M. Liu, X.Y. Qin, Enhanced thermoelectric performance through energy-filtering effects in nanocomposites dispersed with metallic particles, Appl. Phys. Lett. 101 (2012), 132103.
[15] Y. Li, D. Li, X. Qin, X. Yang, Y. Liu, J. Zhang, Y. Dou, C. Song, H. Xin, Enhanced thermoelectric performance through Carrier scattering at heterojunction potentials in BiSbTe based composites with Cu3SbSe4 nanoinclusions, J. Mater. Chem. C 3 (2015) 7045–7052.
[16] C. Li, X. Qin, Y. Li, D. Li, J. Zhang, H. Guo, H. Xin, C. Song, Simultaneous increase in conductivity and phonon scattering in a graphene nanosheets/(Bi2Te3)0.2(Sb2Te3)0.8 thermoelectric nanocomposite, J. Alloys Compd. 661 (2016) 389–395.
[17] R. Liu, L. Xi, H. Liu, X. Shi, W. Zhang, L. Chen, Ternary compound CuInTe2: a promising thermoelectric material with diamond-like structure, Chem. Commun. (Camb) 48 (2012) 3818–3820.
[18] Y. Luo, J. Yang, Q. Jiang, W. Li, Y. Xiao, L. Fu, D. Zhang, Z. Zhou, Y. Cheng, Large enhancement of thermoelectric performance of CuInTe 2 via a synergistic strategy of point defects and microstructure engineering, Nano Energy 18 (2015) 37–46.
[19] P. Puneet, R. Podila, M. Karakaya, S. Zhu, J. He, T.M. Tritt, M.S. Dresselhaus, A.M. Rao, Preferential scattering by interfacial charged defects for enhanced thermoelectric performance in few-layered n-type Bi2Te3, Sci. Rep. 3 (2013) 3212.
[20] X.H. Yang, X.Y. Qin, J. Zhang, D. Li, H.X. Xin, M. Liu, Enhanced thermopower and energy filtering effect from synergetic scattering at heterojunction potentials in the thermoelectric composites with semiconducting nano-inclusions, J. Alloys Compd. 558 (2013) 203–211.
[21] J. Zhang, X. Qin, D. Li, Y. Liu, Y. Li, C. Song, H. Xin, X. Zhu, Enhanced thermoelectric performance of CuGaTe2 based composites incorporated with graphite nanosheets, Appl. Phys. Lett. 108 (2016), 073902.
[22] O. Eibl, K. Nielsch, N. Peranio, F. Völklein, Thermoelectric Bi2Te3 Nanomaterials, John Wiley & Sons, London, 2015.
[23] J.-H. Bahk, A. Shakouri, Enhancing the thermoelectric figure of merit through the reduction of bipolar thermal conductivity with heterostructure barriers, Appl. Phys. Lett. 105 (2014), 052106.
[24] J.K. Lee, M.W. Oh, B. Ryu, J.E. Lee, B.S. Kim, B.K. Min, S.J. Joo, H.W. Lee, S.D. Park, Enhanced thermoelectric properties of AgSbTe2 obtained by controlling heterophases with Ce doping, Sci. Rep. 7 (2017) 4496.
[25] S.I. Kim, K.H. Lee, H.A. Mun, H.S. Kim, S.W. Hwang, J.W. Roh, D.J. Yang, W.H. Shin, X.S. Li, Y.H. Lee, G.J. Snyder, S.W. Kim, Thermoelectrics. Dense dislocation arrays embedded in grain boundaries for high-performance bulk thermoelectrics, Science 348 (2015) 109–114.